



HAL
open science

Terrestrial or oceanic forcing? Water level variations in coastal lagoons constrained by river inflow and ocean tides

Yves Morel, Alexis Chaigneau, Victor Olaègbè Okpeitcha, Thomas Stieglitz, Arnaud Assogba, Thomas Duhaut, Fabien Rétif, Christophe Peugeot, Zacharie Sohou

► To cite this version:

Yves Morel, Alexis Chaigneau, Victor Olaègbè Okpeitcha, Thomas Stieglitz, Arnaud Assogba, et al.. Terrestrial or oceanic forcing? Water level variations in coastal lagoons constrained by river inflow and ocean tides. *Advances in Water Resources*, 2022, 169, pp.104309. 10.1016/j.advwatres.2022.104309 . hal-03780079

HAL Id: hal-03780079

<https://hal.science/hal-03780079>

Submitted on 19 Sep 2022

HAL is a multi-disciplinary open access archive for the deposit and dissemination of scientific research documents, whether they are published or not. The documents may come from teaching and research institutions in France or abroad, or from public or private research centers.

L'archive ouverte pluridisciplinaire **HAL**, est destinée au dépôt et à la diffusion de documents scientifiques de niveau recherche, publiés ou non, émanant des établissements d'enseignement et de recherche français ou étrangers, des laboratoires publics ou privés.

Terrestrial or oceanic forcing? Water level variations in coastal lagoons constrained by river inflow and ocean tides.

Yves Morel^{*1}, Alexis Chaigneau^{1,2,3}, Victor Olaègbè Okpeitcha^{4,3,2}, Thomas Stieglitz⁵, Arnaud Assogba², Thomas Duhaut¹, Fabien Rétif⁶, Christophe Peugeot⁷, Zacharie Sohou²

Abstract

The study concerns the water level (WL) evolution in lagoons under the influence of tides and river fluxes. We derive new approximate analytical solutions of the Stigebrandt (1980) equations and apply them to the Nokoué Lagoon (Benin), a large tropical coastal lagoon fed by substantial river input.

*Corresponding authors

Email addresses: yves.morel@legos.obs-mip.fr (Yves Morel), alexis.chaigneau@ird.fr (Alexis Chaigneau), vokpeitcha@gmail.com (Victor Olaègbè Okpeitcha), stieglitz@cerege.fr (Thomas Stieglitz), (Arnaud Assogba), thomas.duhaut@legos.obs-mip.fr (Thomas Duhaut), fabien.retif@zoho.com (Fabien Rétif), christophe.peugeot@ird.fr (Christophe Peugeot), zsohou@yahoo.fr (Zacharie Sohou)

¹LEGOS, Université de Toulouse, CNES, CNRS, IRD, UPS, Toulouse 31400, France

²Institut de Recherches Halieutiques et Océanologiques du Bénin (IRHOB), Cotonou, Benin

³International Chair in Mathematical Physics and Applications (ICMPA, UNESCO Chair)/University of Abomey-Calavi, Cotonou, Benin

⁴Laboratoire d'Hydrologie Appliquée (LHA), Institut National de l'Eau (INE), African Centre of Excellence for Water and Sanitation (C2EA), University of Abomey Calavi, Benin

⁵Aix-Marseille Université, CNRS, IRD, INRAE, Coll France, CEREGE, Aix-en-Provence, France

⁶RETIF FABIEN PHILIAN, Montferrier sur Lez, France

⁷HSM, IRD, Univ. Montpellier, CNRS, IMT, Montpellier, France

We show the solutions accurately predict the mean WL and tide amplitude. In particular the non linear combination of the spring-neap tidal cycle and river inflow gives rise to a strong fortnightly variation of the mean WL. The analytical solutions are used to explain this phenomenon. We also calculate the phase shift between the ocean and the lagoon tides and the asymmetry of the ebb and flood tide duration in the lagoon. The asymmetry first increases with the river flux but reduces above a critical flux before becoming symmetric again at river flood peaks.

Finally, the analytical solutions are inverted to estimate the net river fluxes entering the Nokoué Lagoon, where no observations are available for rivers but for which we have high frequency observations of the lagoon water level for 2 years. The model is calibrated using few available flux observations in the channel connecting the lagoon to the ocean. Realistic river fluxes are estimated. We subsequently calculate the lagoon WL variations using the simplified model forced with the recalculated river fluxes and tidal forcing from an ocean tide model. The solution accurately represents the observations over the 2 year time period of the study. We conclude that this simple model is able to represent the complex interaction of tides and river fluxes, and its influence on the low frequency WL variations of coastal lagoons.

Key words: Lagoon, water level, tide, river flux.

1. Introduction

Located in the continent-ocean aquatic continuum, coastal lagoons are among the most biologically productive environments and deliver valuable ecosystem services and socioeconomic benefits (e.g. Newton et al., 2018). In

Benin, Nokoué Lagoon is the largest continental water body of the country and is exploited by more than 12000 artisanal fishermen (Latifou et al., 2020). This coastal lagoon, which provides more than 65% of the national fish production, is very important for the local communities not only because it generates income but also because it is a large source of protein for the whole population (FAO, 2008) and ensures part of the Benin's food security. This large natural aquatic space is also strongly anthropized : it hosts the largest lacustrine villages in the sub-region and is surrounded by large urban centers with a combined population of more than 1.5 million people (Cotonou, Abomey-Calavi, etc., see Fig. 1) . While these coastal populations benefit from various ecosystem services provided by the lagoon (Djihouessi et al., 2017), they are also exposed to natural hazards, particularly flooding. Indeed, Benin is largely under the influence of the African monsoon associated with the seasonal meridional migration of the intertropical convergence zone, which leads to annual rainfall totals of 1000 to 1300 mm in the country (Le Barbé et al., 1993). These intense rainfalls, which are maximum in April-June in southern Benin (August-September in northern Benin), infiltrate and/or run off and reach the southern part of Benin, mainly through the Ouémé and Sô watersheds, which form a vast delta and lead to the Nokoué Lagoon (Le Barbé et al., 1993). Although the net river flow considerably varies from the dry to the wet season, an exact quantification remains uncertain as rivers are not regularly gauged. Previous studies report river flow variations from a few tens of m^3/s in the dry season to 1000 m^3/s in the wet season (Chaigneau et al., 2022; Le Barbé et al., 1993; Djihouessi and Aina, 2018; Lawin et al., 2019). This strong seasonal variation of freshwater

inflow results in a complete seasonal reversal of the salinity and ecosystem of the lagoon (Lalèyè et al., 2003; Okpeitcha et al., 2022) and can lead to major floodings. In the wet season, the water level (WL) in the rivers increases by several meters (Le Barbé et al., 1993) and in the Nokoué Lagoon, the average depth increases from 1.3 m in low-water period to 2.1 m in flood period (Chaigneau et al., 2022). Interannual variations in rainfall can lead to exceptional flood with disastrous impacts for local populations. For instance, in 2010, the unprecedented flooding of the Ouémé River resulted in about 100 deaths, the displacement of 700,000 people, the destruction of more than 50,000 homes, and the loss of 130,000 hectares of crops and 80,000 heads of livestock (World-Bank, 2011; Ahouangan et al., 2014; Biao, 2017). Similarly, in 2019, a major flood was less intense but extended over several weeks (Chaigneau et al., 2022), causing significant damages and affecting tens of thousands of households (Chaigneau et al., 2022). Thus, in order to protect the population and avoid these numerous human and material damages, it is necessary to set up early warning systems for floods, based on both continuous observations and numerical models.

Recently, Chaigneau et al. (2022) described the main patterns of the WL variations observed in Nokoué Lagoon, based on 2 years of high-frequency WL measurements. They showed that the lagoon, constrained by tide and river flow, is tidally choked. As a result, ocean tide is strongly attenuated through the long (4 km) and narrow (300 m) Cotonou channel (see Figure 1a), but fortnightly variations of the mean WL of ± 10 cm is observed in the lagoon. They concluded that, to be realistic and in contrast to what is generally used, a flood forecasting system for southern Benin has to take into

account tide forcing.

The main purpose of this study is thus to set up a numerical model that realistically reproduces the WL fluctuations observed in Nokoué Lagoon. For this, we will use a relatively simple theoretical model, initially developed by Stigebrandt (1980) (see also Hill, 1994) which has been widely used to study choked lagoons (e.g. Hill, 1994; Rydberg and Wickbom, 1996; Albrecht and Vennell, 2007; MacMahan et al., 2014). However, the novelty of the present study is to propose new analytical solutions taking into account both the river and tide fluxes. We derive approximate analytical solutions for the mean WL and the tidal amplitude in a lagoon. While the analytical solutions are valid for any choked lagoon characteristics, we validate the analytical solutions for a configuration representative of the Nokoué Lagoon. The physics explaining the observed WL characteristics is then discussed, focusing on tidal amplitude and variations of the mean WL between neap and spring tides. Finally, we use an inversion of the model to estimate variations in river discharge from the observed mean WL fluctuations in the lagoon and the ocean tide amplitude.

2. Data and model

2.1. Nokoué Lagoon

Figure 1 (lower panel) represents 2 years of WL⁸ variation of the Nokoué Lagoon (η_{lag}). These observations, acquired at high-frequency (every 20 *min.*) by an Onset HOBO U20L-01 pressure sensor installed in the south of the lagoon, were analyzed in details by Chaigneau et al. (2022). Here, very

⁸Note that in the following, the WL refers to the free surface and is calculated with respect to a state at rest

high-frequency signals ($< 5 \text{ hr}$) have been filtered out using a wavelet reconstruction technique (see Chaigneau et al., 2022, for details). The main observed features are the low-frequency seasonal variations associated with river fluxes to the lagoon and the high frequency signal associated with tide. Also visible is a 14 – *day* period, associated with neap-spring tide cycle, but whose signature appears in the mean WL of the lagoon. (Hill, 1994) described such a feature as the result of nonlinear effects associated with the tidal WL variations within the channel. We will see that, in the present case, it is associated with nonlinear interactions between tide and river fluxes.

In addition to the WL observations, 14 field campaigns have been carried out across the Cotonou channel (see Fig.1 upper panel) between February 2018 and January 2020. These campaigns were dedicated to measure the fluxes during $\simeq 13$ consecutive hours using an acoustic Doppler current profiler (ADCP Teledyne RDI WorkHorse 1200-kHz), mounted on the side of a small wooden boat. Each field campaigns consisted on more than 100 repetitive cross-sections, during which vertical profiles of velocity data were collected at 1s intervals using WinRiver II software (RDI Teledyne) with GPS positioning and bottom-tracking. For each section, these profiles were integrated throughout the wet cross-section to obtain inflow-outflow flux estimates during one semi-diurnal tidal cycles. The obtained fluxes are driven by both the tide and the river discharge. The mean flux is associated with the net river discharge into the lagoon. During the dry season, it is weak (a few tens of m^3/s) and difficult to evaluate because the tide signal is very strong (up to $500 m^3/s$, see Okpeitcha et al., 2022) and because the observations does not cover a sufficient time period (observations of the channel

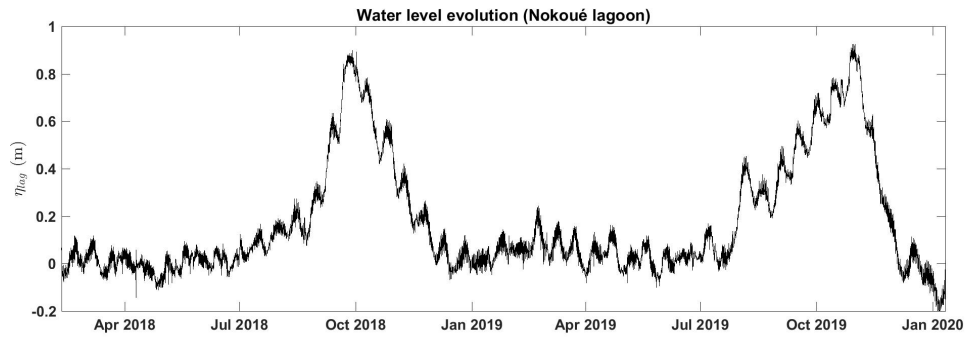
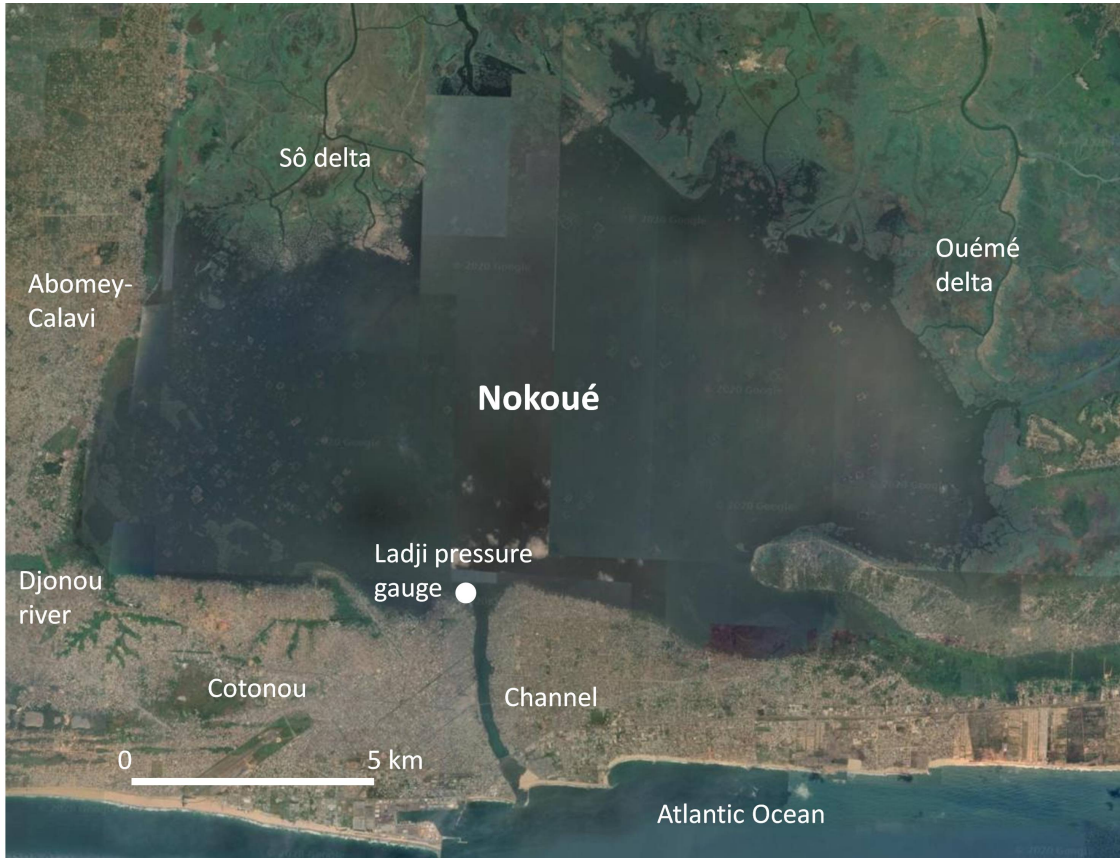


Figure 1: Satellite view of the Nokoué Lagoon in Benin (upper panel) and observed variations of the WL in the southern part of the lagoon (see white dot above), from February the 10th 2018 to February the 10th 2020 (lower panel).

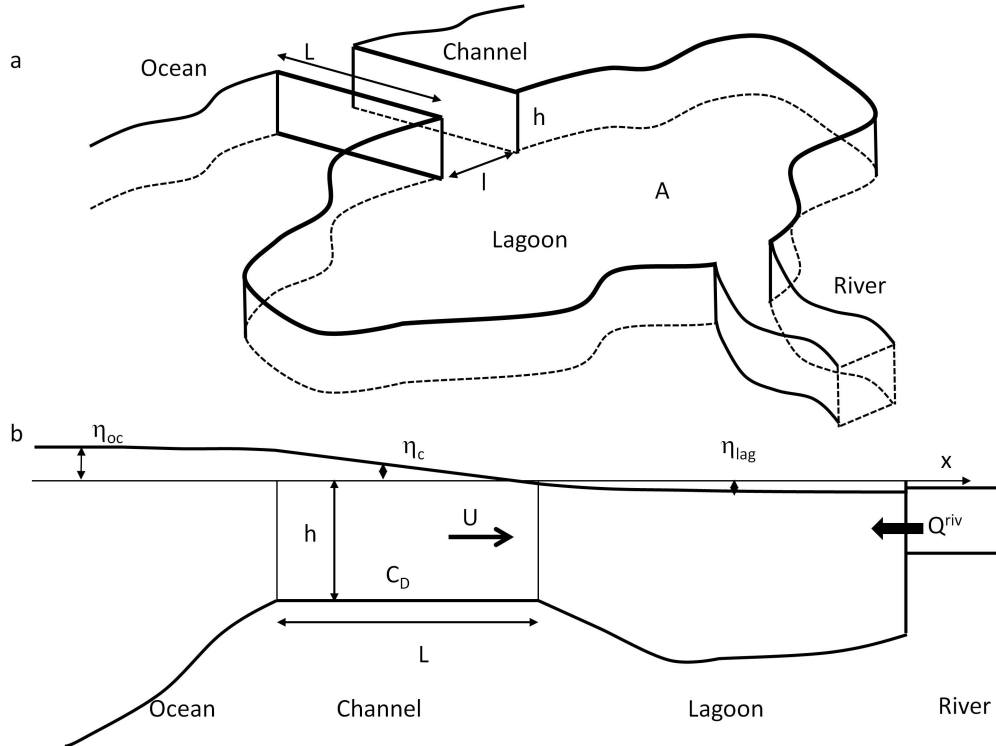


Figure 2: General configuration. General view (a) and side view (b).

are not possible during the night, which limits the time period of observation to a maximum of 13-14 hours during the day). When the river discharge becomes very large, the effect of tide on mean fluxes within the channel diminishes and the net flux can be evaluated with little error from the 13-14h data available (see section 5.2).

2.2. Simplified model

Figure 2 presents the general schematic configuration of the theoretical model of a choked lagoon. In the open ocean, sea surface height (η_{oc}) is controlled by tides, and is independent of the channel or lagoon dynamics and

geometry. As initially proposed by Stigebrandt (1980) (see also Hill, 1994; MacMahan et al., 2014), the WL in the lagoon (η_{lag}) is considered uniform and controlled by the channel and river fluxes related to tides and freshwater discharge, respectively. The channel controls the exchange between the lagoon and the open ocean. The flux in the channel is constrained by geometrical characteristics of the channel (length, width, depth) and bottom friction, inducing tidal choking. Under the simplifying assumptions given above, the governing equations are (Stigebrandt, 1980; Hill, 1994; MacMahan et al., 2014)

$$A \frac{d\eta_{lag}}{dt} = U (h + \eta_C) l + Q^{riv} \quad (1a)$$

$$\frac{C_D |U| U}{h + \eta_C} = g \frac{\eta_{oc} - \eta_{lag}}{L} \quad (1b)$$

$$\eta_C = \frac{\eta_{oc} + \eta_{lag}}{2} \quad (1c)$$

where Eq. 1a is the conservation of volume of the lagoon and Eq. 1b is derived from the equilibrium between bottom friction (quadratic form) and pressure gradient in the channel. Here, Q^{riv} is the total river flux, A is the lagoon area ($A \simeq 170 \text{ km}^2$ for Nokoué Lagoon, Djihouessi and Aina (2018)), h , L , l are the height, length and width of the channel (see Fig. 2), C_D is the bottom friction, η_C is the elevation of the surface in the channel (usually assumed to vary linearly from η_{oc} to η_{lag} along the channel, but neglected in the present study given the channel depth), U is the velocity in the channel and is positive when directed toward the lagoon (and $|U|$ is its absolute value), g is gravity. The water flux is here assumed constant along the channel and represented by an evaluation of U at the center of the

channel (Eq. 1b and 1c).

Rearrangement of the set of equations 1 results in the final nonlinear equation for η_{lag} as a function of Q^{riv} and η_{oc}

$$\frac{d\eta_{lag}}{dt} = \Gamma \frac{\eta_{oc} - \eta_{lag}}{\sqrt{|\eta_{oc} - \eta_{lag}|}} + \frac{Q^{riv}}{A} \quad (2)$$

where Γ is the choking coefficient (Stigebrandt, 1980) related to the characteristics of the channel

$$\Gamma = \frac{l}{A} \sqrt{\frac{g (h + (\eta_{oc} + \eta_{lag})/2)^3}{C_D L}} \quad (3)$$

If the WL fluctuations (η_{oc} and η_{lag}) are small compared to the channel depth, gamma reduces to:

$$\Gamma \simeq \frac{l}{A} \sqrt{\frac{g h^3}{C_D L}} \quad (4)$$

Additional processes (such as the presence of bridge pillars or hydraulic constrictions at the entrance of the channel) can be taken into account, as long as they can be parameterized similarly to frictional effects (Stigebrandt, 1992). Also note that both the geometrical and hydrodynamic characteristics can vary along and across channels. Evaluating Γ from Eq. 4 using simple geometric parameters is thus subject to caution. In fact, Γ , can be viewed as a coefficient that characterizes the bulk dissipative effects of the channel. In this case, Eq. 2 is still valid but Γ is more complex and depends on other parameters (see Stigebrandt, 1980, 1992). However, it is not necessary to know the exact expression for Γ , only its value is of interest and can be evaluated from observations. In this study, we consider that Γ is a constant parameter representing the average dissipative effect of the channel. Based on the ADCP data acquired in the Cotonou Channel, we estimate a value

of $\Gamma \simeq 7.10^{-6} \text{ m}^{1/2}/\text{s}$ that accounts for the observed variations of WL in the lagoon (see section 5). This value is thus used in the next sections dealing with sensitivity studies and a simplified configuration. Given Γ , A , Q^{riv} and η_{oc} , Eq. 2 determines the lagoon WL variations.

3. Numerical results

3.1. Nonlinear tide and river flux interactions

We first consider simplified configurations with simplified forcings to analyze the interactions between tidal and river forcings. We here assume that the ocean tide is purely sinusoidal and given by

$$\eta_{oc} = \delta\eta_{oc}^{tide} \sin \omega t \quad (5)$$

Off Cotonou, the tide is dominated by the M2 semi-diurnal component, associated with the gravitational forces exerted by the Moon. Its period is half a lunar day ($\omega^{M2} \simeq 1.4 \cdot 10^{-4} \text{ s}^{-1}$) and its typical amplitude in sea-level variations is $\delta\eta_{oc}^{tide} \simeq 0.5 \text{ m}$ (Chaigneau et al., 2022). A spring-neap tidal cycle and diurnal variations results in a range of variation of $\delta\eta_{oc}^{tide}$ of $[0.2, 0.8] \text{ m}$ (Chaigneau et al., 2022).

We also assume that the WL in the lagoon can be written

$$\eta_{lag} = \overline{\eta_{lag}} + \delta\eta_{lag}^{tide} s(\omega t + \phi) \quad (6)$$

where $\delta\eta_{lag}^{tide}$ is the tide amplitude in the lagoon, ϕ its phase, $\overline{\eta_{lag}}$ is the mean level of the lagoon and s is a periodic function with zero mean.

Q^{riv} significantly varies between the dry and the wet seasons. In order to determine the sensitivity of the WL variation of the Nokoué Lagoon to

the river discharge, several simplified experiments are now performed, where the river discharge Q^{riv} is either constant in time or follows analytically prescribed variations.

We have solved Eq. 2 numerically for a range of scenarios, with $\Gamma = 7.10^{-6} m^{1/2}/s$, $A = 1.7 \cdot 10^8 m^2$ and varying values for $\delta\eta_{oc}^{tide}$ and Q^{riv} . Figure 3 represents solutions obtained for $Q^{riv} = 0$ (no river discharge), $Q^{riv} = 500 m^3/s$ and $Q^{riv} = 1000 m^3/s$ (constant river flux) and for $\delta\eta_{oc}^{tide} = 0$ (no tide) and $\delta\eta_{oc}^{tide} = 0.5 m$. Without river flux and only taking into account the oceanic tide, the lagoon WL exhibits near sinusoidal variations (thick black plain curve), with zero mean and an amplitude $\delta\eta_{lag}^{tide} \simeq 4.5 cm$. This experiment clearly shows that the tide amplitude is strongly weakened from the ocean (50 cm) to the lagoon (4.5 cm) due to the choking effect of the Cotonou channel. Without tide but with a river flux of $Q^{riv} = 500 m^3/s$, the lagoon WL is constant reaching a mean level $\overline{\eta_{lag}} \simeq 17 cm$ (dashed blue curve). When both the tide and river flux are considered (thick plain blues curves), there are important differences:

- the mean lagoon level increases significantly and reaches $\overline{\eta_{lag}} \simeq 34 cm$.
The presence of the tide, even though it does not generate a mean level in the lagoon by itself, strongly increases the impact of the river flux on the mean level.
- the high frequency tidal signal is also very different. The amplitude is reduced to $\delta\eta_{lag}^{tide} \simeq 3.4 cm$ and the signal exhibits a strong asymmetry characterized by longer ebb and shorter flood phases.

The solutions obtained for $Q^{riv} = 1000 m^3/s$ and for $\delta\eta_{oc}^{tide} = 0$ and

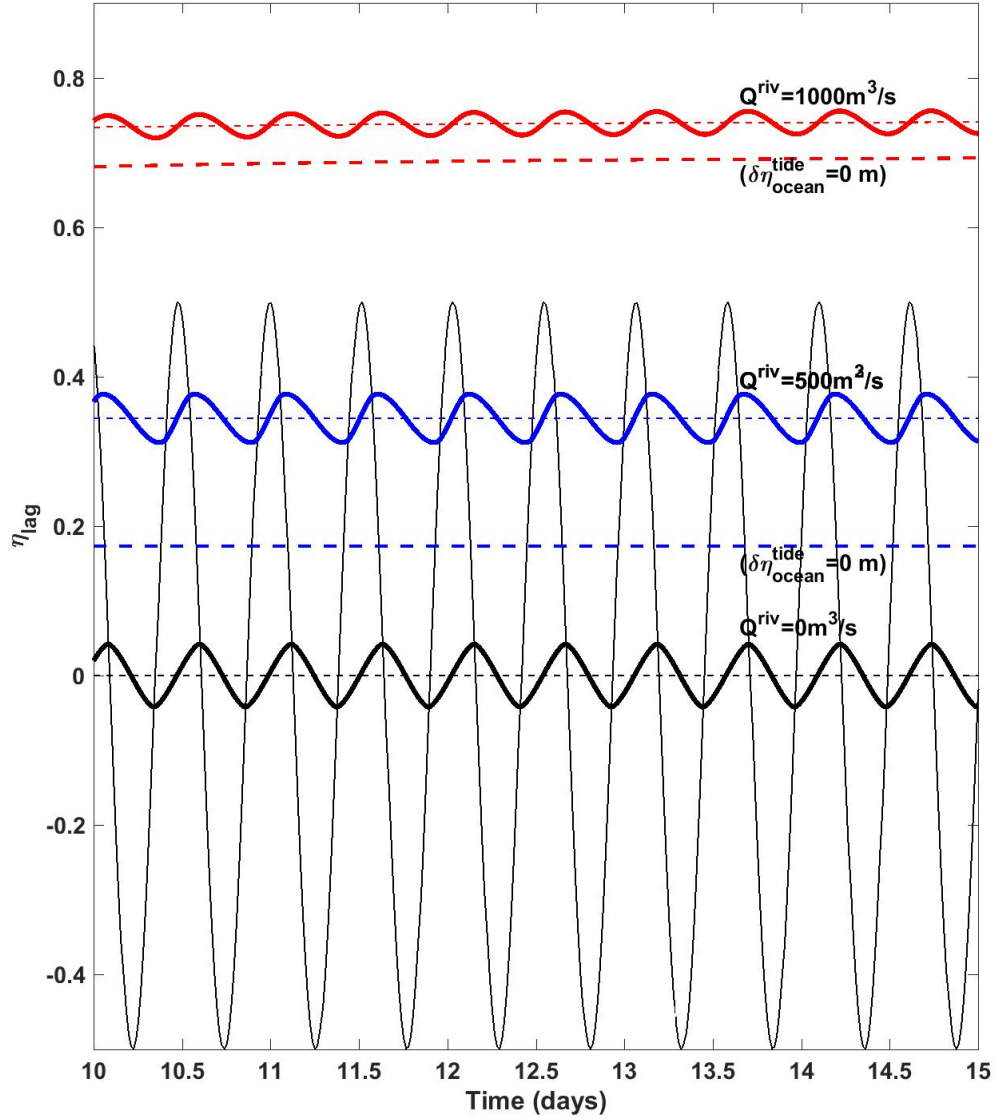


Figure 3: WL variations in the lagoon as a function of time, for $Q^{riv} = 0 \text{ m}^3/\text{s}$ (black), $Q^{riv} = 500 \text{ m}^3/\text{s}$ (blue) and $Q^{riv} = 1000 \text{ m}^3/\text{s}$ (red). For each river flux, we calculate η_{lag} with an ocean tide of $\delta\eta_{oc}^{tide} = 0.5 \text{ m}$ (thick plain curves) and without tide ($\delta\eta_{oc}^{tide} = 0 \text{ m}$, thick dashed curves). η_{oc} is also represented (thin black plain line) as well as the mean lagoon level $\overline{\eta_{lag}}$ (dashed line).

$\delta\eta_{oc}^{tide} = 0.5 \text{ m}$ (Fig. 3, red curves) show that the mean WL in the lagoon increases to $\overline{\eta_{lag}} \simeq 69 \text{ cm}$ without tide and $\overline{\eta_{lag}} \simeq 74 \text{ cm}$ with the M2 tide. The impact of tide on the mean WL is thus much smaller for $Q^{riv} = 1000 \text{ m}^3/\text{s}$ than for $Q^{riv} = 500 \text{ m}^3/\text{s}$. A river discharge of $Q^{riv} = 1000 \text{ m}^3/\text{s}$ also further damped the tide amplitude to $\delta\eta_{lag}^{tide} \simeq 1.6 \text{ cm}$, and the ebb and flood phases now have similar durations.

To conclude, these simplified experiments reproduce well the nonlinear interaction between the high frequency forcing associated with tides and the low frequency forcing associated with river discharge, both on the mean WL and on the tidal signal in the lagoon. Similar interactions are known to occur in estuaries. We further investigate these processes in section 4.

3.2. Effect of spring/neap tide cycle and variable river flux

Here, we consider the fortnightly variability associated with spring-neap tidal cycles taking into account both the M2 and S2 tidal components, the latter being associated with the gravitational forces exerted by the Sun:

$$\eta_{oc} = \eta_{oc}^{M2} \sin \omega^{M2}t + \eta_{oc}^{S2} \sin \omega^{S2}t \quad (7)$$

with $\eta_{oc}^{M2} = 0.5 \text{ m}$, $\omega^{M2} = 1.406 \cdot 10^{-4} \text{ s}^{-1}$ and $\eta_{oc}^{S2} = 0.2 \text{ m}$, $\omega^{S2} = 1.451 \cdot 10^{-4} \text{ s}^{-1}$.

We also use a more realistic, time varying, river flux taken as a Gaussian function $Q^{riv} = Q_{max}^{riv} \exp(-t^2/2T_Q^2)$ whose maximum reaches $Q_{max}^{riv} = 1000 \text{ m}^3/\text{s}$ after 180 days and extending over $T_Q = 50 \text{ days}$ (see Fig. 4 a).

Figure 4 shows the result of the integration of Eq. 2 over 365 days with these forcings. The sea surface height η_{oc} exhibits a regular spring-neap tidal cycle of 14 days, with a high frequency (M2) tide signal varying from

a minimum of $\delta\eta_{oc}^{tide} = 0.3 \text{ m}$ to a maximum of $\delta\eta_{oc}^{tide} = 0.7 \text{ m}$ (Fig. 4b), typical of what is observed off Cotonou.

The mean WL in the lagoon significantly varies during the simulation. When the river flux is close to zero, the WL exhibits sinusoidal variations around 0 with an amplitude varying from $\delta\eta_{lag}^{tide} = 3.4 \text{ cm}$ during neap tides to $\delta\eta_{lag}^{tide} = 5.2 \text{ cm}$ during spring tides (Fig. 5). When the river flux becomes significant (around $t = 50 \text{ days}$ or so) the lagoon WL is strongly modified. As can be expected from section 3.1, the river flux establishes a mean WL (Fig. 4c, thick solid line) that is strongly affected by the tide amplitude. The mean WL is always above the WL reached without tide (Fig. 4c, dashed line). However, the amplification rate is first very strong (note that at $t = 100 \text{ days}$ the mean WL remains weak in the simulation without tide, but reaches about 0.17 m when tides are taken into account) but is reduced above a certain river flux. Another striking effect is that the spring-neap tidal cycles have an impact on the mean WL in the lagoon. The spring-neap tidal cycle signature on the mean WL also reaches a maximum for intermediate river fluxes.

The high frequency tidal signal in the lagoon is also affected. Figure 5a (black dashed curve) shows that the tidal signal is strongly damped with increasing river discharge. When the river flux reaches its maximum value, the tide amplitude in the lagoon varies from $\delta\eta_{lag}^{tide} = 1 \text{ cm}$ to $\delta\eta_{lag}^{tide} = 2.5 \text{ cm}$ during a spring-neap tidal cycle.

In the following sections, we propose analytical developments and approximate solutions (section 4.2) to explain the numerical results presented above and the physics of the nonlinear effects (section 4.3).

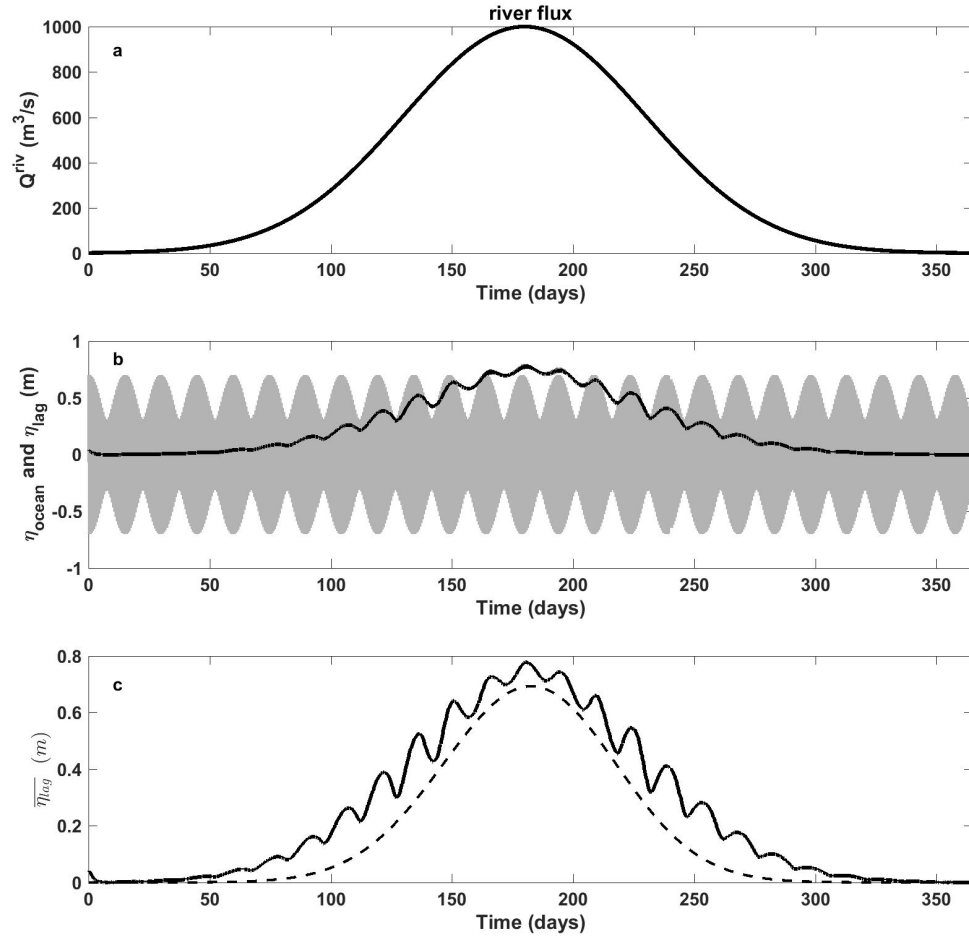


Figure 4: Panel a: Variation of the river flux $Q^{riv} = Q_{max}^{riv} \exp(-t^2/2T_Q^2)$ ($Q_{max}^{riv} = 1000 \text{ m}^3/s$ is reached after 180 days and $T_Q = 50 \text{ days}$). Panel b: variation of the surface elevation in the ocean (η_{oc} , gray curve) and in the lagoon (η_{lag} , black curve) as a function of time. Panel c: mean WL in the lagoon (running mean over 1 days). The mean WL with the same river flux but no tide is plotted as a dashed line.

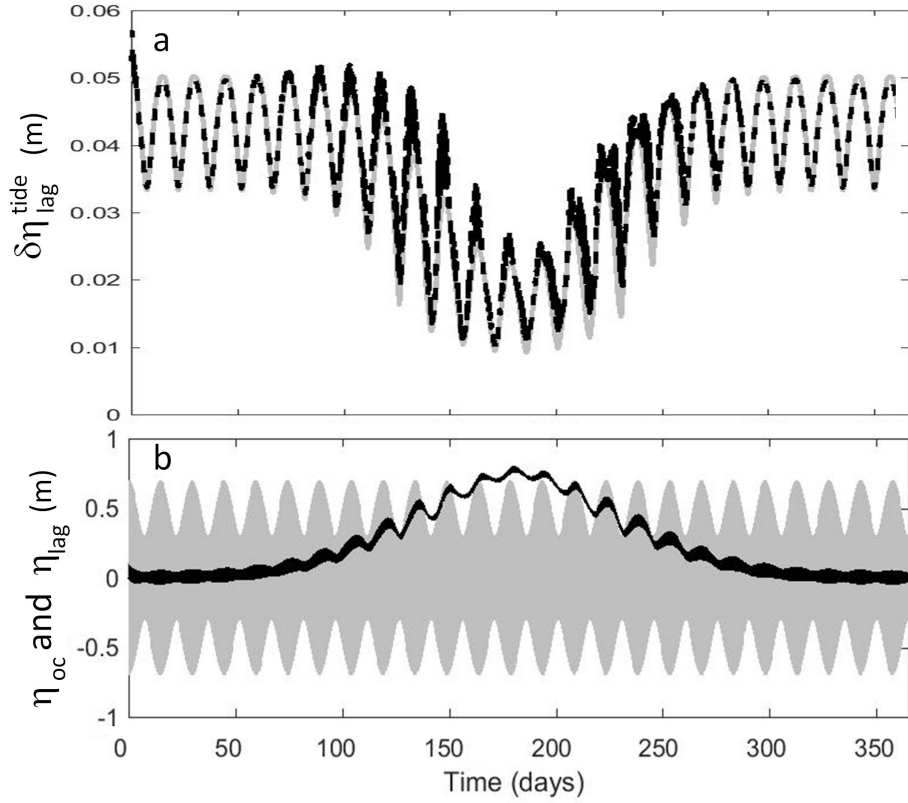


Figure 5: Evolution of tide amplitude $\delta\eta_{lag}^{tide}$ (in m) in the lagoon (calculated using maximum and minimum of elevation over a tide period, panel a). The black dashed curve represents the results from the numerical simulation. The gray curve is the prediction of the analytical formula Eq. 11. Variation of the surface elevation in the ocean (η_{oc} , gray curve, panel b) and in the lagoon (η_{lag} , black curve) have been added for comparison.

4. Theoretical and physical analysis

4.1. Steady state

For a constant river flux and an ocean with no tidal variation, an equilibrium regime can be achieved between bottom friction and river flux, with a mean level $\overline{\eta_{lag}^{riv}}$. Equation 2 gives

$$\Gamma \sqrt{\overline{\eta_{lag}^{riv}}} = \frac{Q^{riv}}{A} \quad (8)$$

which yields

$$\overline{\eta_{lag}^{riv}} = \left(\frac{Q^{riv}}{\Gamma A} \right)^2 \quad (9)$$

$\overline{\eta_{lag}^{riv}}$ is the mean WL in the lagoon obtained without tide and a constant (or slowly varying) river flux.

4.2. Effect of tidal forcing

4.2.1. Mean WL in the lagoon

Here we assume that the ocean sea surface height is given by Eq. 5. The tide amplitude is allowed to vary (considering the spring-neap tidal cycle for instance) but its evolution is assumed slow in comparison with the timescale of the adjustment in the lagoon. The previous numerical experiments show that the WL in the lagoon is the superposition of a constant mean level and a tidal signal (see Eq. 6) and of course $\overline{\eta_{lag}} = \overline{\eta_{lag}^{riv}}$ when the tide amplitude $\delta\eta_{oc}^{tide} = 0$.

In appendix A we show that an approximate solution for the mean level

is

$$\overline{\eta}_{lag} = F^{-1}\left(\sqrt{\frac{\overline{\eta}_{lag}^{riv}}{\delta\eta_{oc}^{tide}}}\right) \delta\eta_{oc}^{tide} \simeq \begin{cases} 1.2 \sqrt{\overline{\eta}_{lag}^{riv} \delta\eta_{oc}^{tide}} & \text{if } \sqrt{\overline{\eta}_{lag}^{riv}/\delta\eta_{oc}^{tide}} \rightarrow 0 \\ \overline{\eta}_{lag}^{riv} & \text{if } \sqrt{\overline{\eta}_{lag}^{riv}/\delta\eta_{oc}^{tide}} \rightarrow \infty \end{cases} \quad (10)$$

$\overline{\eta}_{lag}$ depends on the river flux and the ocean tide amplitude through a nonlinear function F^{-1} (see appendix A for an expression of the function F), but is independent of the tide frequency ω (as long as it can be considered high frequency in comparison with the river flux evolution) and, in the present model, it is zero when the river flux is zero. Figure 6 represents the function F^{-1} and its approximations.

When the river flux becomes large (in comparison with the tide amplitude, this requires $\sqrt{\overline{\eta}_{lag}^{riv}/\delta\eta_{oc}^{tide}} \geq 1.5$, or so), $F^{-1}(\sqrt{\overline{\eta}_{lag}^{riv}/\delta\eta_{oc}^{tide}}) \simeq \overline{\eta}_{lag}^{riv}/\delta\eta_{oc}^{tide}$ (thin and thick dashed line in Fig. 6) and $\overline{\eta}_{lag} \simeq \overline{\eta}_{lag}^{riv}$: the mean level becomes close to the equilibrium level obtained without tide, as expected. Also $\overline{\eta}_{lag}$ is always above $\overline{\eta}_{lag}^{riv}$: the tide always increases the mean level in the lagoon.

For large oceanic tides or weaker river fluxes ($\sqrt{\overline{\eta}_{lag}^{riv}/\delta\eta_{oc}^{tide}} \leq 0.8$, or so), $F^{-1}(\sqrt{\overline{\eta}_{lag}^{riv}/\delta\eta_{oc}^{tide}}) \simeq 1.2 \sqrt{\overline{\eta}_{lag}^{riv}/\delta\eta_{oc}^{tide}}$ (thick strait dashed line in Fig. 6) and $\overline{\eta}_{lag} \simeq 1.2 \sqrt{\overline{\eta}_{lag}^{riv} \delta\eta_{oc}^{tide}}$. The tide amplitude strongly modulates the mean WL of the lagoon and amplifies the effect of the river flux. In these circumstances, the mean WL of the lagoon is also strongly affected by the spring-neap tidal cycles.

In addition, for a given tide amplitude $\delta\eta_{oc}^{tide}$, the amplification of the tidal effect can be estimated as $\Delta\overline{\eta}_{lag} \simeq 1.2 \sqrt{\overline{\eta}_{lag}^{riv} \delta\eta_{oc}^{tide}} - \overline{\eta}_{lag}^{riv}$, whose maximum is reached when $\sqrt{\overline{\eta}_{lag}^{riv}/\delta\eta_{oc}^{tide}} = 0.6$ and the maximum increase due to the tide is thus simply proportional to the tide amplitude $\Delta\overline{\eta}_{lag} \simeq 0.36 \delta\eta_{oc}^{tide}$.

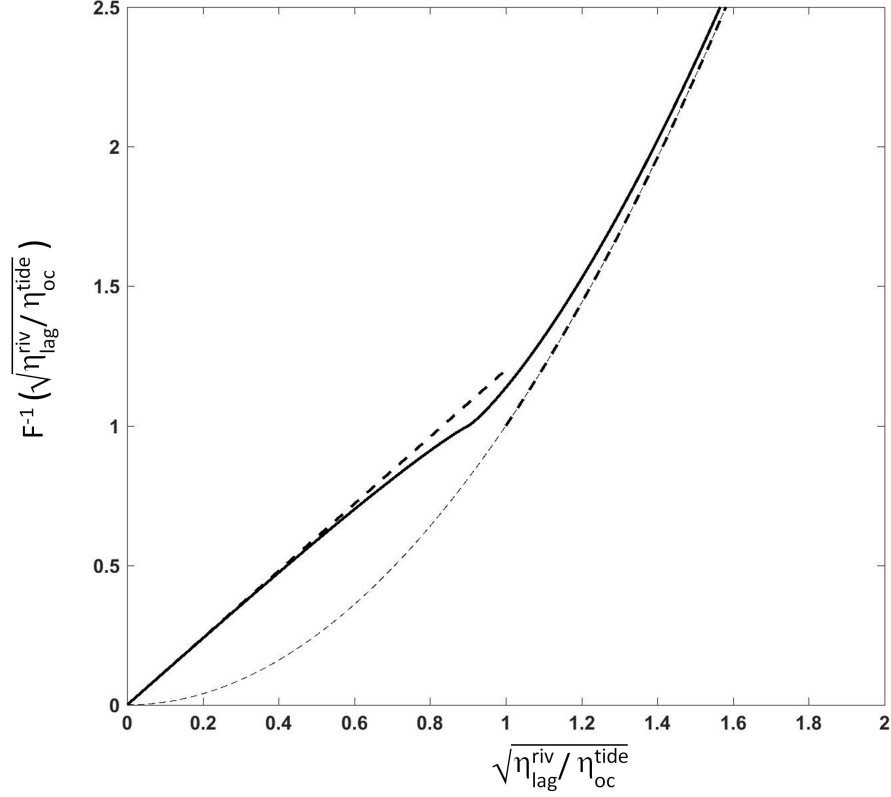


Figure 6: Function F^{-1} given by Eq. 20 (plain thick line) and its approximate forms $F^{-1}(\sqrt{\eta_{lag}^{riv}/\delta\eta_{oc}^{tide}}) = 1.2 \sqrt{\eta_{lag}^{riv}/\delta\eta_{oc}^{tide}}$ and $F^{-1}(\sqrt{\eta_{lag}^{riv}/\delta\eta_{oc}^{tide}}) = \overline{\eta_{lag}^{riv}}/\delta\eta_{oc}^{tide}$ (see appendix A) extended respectively to $[0, 1]$ and $[1, \infty]$ (dashed lines). The asymptotic form for large values corresponds to large river flux for which $\overline{\eta_{lag}} \simeq \overline{\eta_{lag}^{riv}}$. It has also been extended to small values (thin dashed line) to show that, in all cases, the effect of the tide always increases the equilibrium level of the lagoon.

This shows again that the spring-neap cycle has drastic consequences on the mean level of the lagoon.

The previous analytical results are generally valid for choked lagoons of any size, tidal regime and river inflow. Applying them to Nokoué Lagoon, for which $\Gamma = 7.10^{-6} \text{ m}^{1/2}/\text{s}$, $A = 1.7 \cdot 10^8 \text{ m}^2$ and the mean tide amplitude is $\simeq 0.5 \text{ m}$ (see section 3.1), the maximum effect of tide is reached for a river flux of $Q^{riv} \simeq 500 \text{ m}^3/\text{s}$ and is about $\Delta \overline{\eta}_{lag} \simeq 0.36 \delta \eta_{oc}^{tide} \simeq 0.18 \text{ m}$, very close to what is found numerically (17 cm, see section 3.1 and Fig. 3). For $Q^{riv} \simeq 1000 \text{ m}^3/\text{s}$, we get $\sqrt{\overline{\eta}_{lag}^{riv}/\delta \eta_{oc}^{tide}} \simeq 1.2$ and the effect of tide is reduced, explaining Figs. 3 and 4.

In section 3.2, we considered the spring-neap cycle with amplitudes varying between 0.3 m and 0.7 m (Fig. 4b). The mean tide is again 0.5 m, so the maximum effect of tide is again expected to be reached for $Q^{riv} \simeq 500 \text{ m}^3/\text{s}$, reached around $T = 140 \text{ days}$, and the WL difference between neap and spring tides is $\Delta \overline{\eta}_{lag}(spring - neap) \simeq 0.36 \delta \eta_{oc}^{tide}(spring - neap) \simeq 0.36 \times 0.4 \simeq 14 \text{ cm}$ which is in agreement to what is found in Fig. 4c.

Figure 7, left panel, represents the mean lagoon WL $\overline{\eta}_{lag}$ as a function of both the ocean tide amplitude $\delta \eta_{oc}^{tide}$ and the river discharge Q^{riv} . The difference of the mean WL with and without tides $\Delta \overline{\eta}_{lag} \simeq 1.2 \sqrt{\overline{\eta}_{lag}^{riv}} \delta \eta_{oc}^{tide} - \overline{\eta}_{lag}^{riv}$ is always positive (right panel). The maximal amplification for a specific river flux Q^{riv} is clearly visible and can reach $\simeq 25 \text{ cm}$ for the parameter range considered in previous sections (identified by the dashed rectangle in Fig. 7). Moreover tides have a significant impact, with an increase of at least 10 cm over most of the parameter range, as soon as the river flux is above $100 \text{ m}^3/\text{s}$ or so.

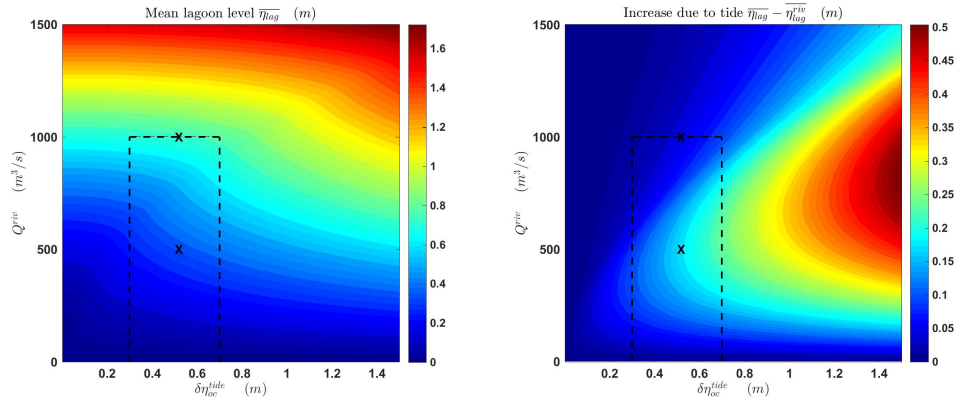


Figure 7: Left panel: mean lagoon WL $\overline{\eta_{lag}}$ given by Eq. 10 as a function of both the ocean tide amplitude $\delta\eta_{oc}^{tide}$ and the river flux Q^{riv} and for the Nokoué Lagoon characteristics: $\Gamma = 7.10^{-6} m^{1/2}/s$, $A = 1.7 \cdot 10^8 m^2$. Right panel: increase of lagoon mean level due to tide as a function of both the ocean tide amplitude $\delta\eta_{oc}^{tide}$ and the river flux Q^{riv} . The experiments presented in section 3.1 are indicated by 'X'. The experiment presented in section 3.2 with variable tide amplitude and variable river fluxes are delimited by the dashed lines.

To conclude, the analytical results show that, when the river flux is not zero, the WL of the lagoon increases at a rate that also depends on the tide amplitude in the ocean: the stronger the tide, the larger the increase. The analytical results we found explains the effects observed in section 3, as a result of nonlinear interaction between high frequency forcing of the tide and low frequency forcing of river inflow.

4.2.2. Tide signal in the lagoon

In appendix A we show that the tide amplitude in the lagoon can be estimated by

$$\delta\eta_{lag}^{tide} \simeq \frac{\Gamma \sqrt{\delta\eta_{oc}^{tide}}}{\omega} G(\overline{\eta}_{lag}/\delta\eta_{oc}^{tide}) \quad (11)$$

where ω is the main tidal frequency (here associated with M2), $\overline{\eta}_{lag}$ is given by Eq. 10 and G is a damping function depicted in Fig. 8. The ratio of the lagoon tide amplitude to the oceanic one ($\delta\eta_{lag}^{tide}/\delta\eta_{oc}^{tide}$) is maximum when there is no river flux and is $\simeq 1.2 \Gamma \sqrt{\delta\eta_{oc}^{tide}}/\omega$.

As shown in Fig. 8, G is a decreasing function so that the tide amplitude ratio is reduced with increasing river flux. For $\overline{\eta}_{lag}/\delta\eta_{oc}^{tide} \leq 0.5$ the additional choking effect of the river flux remains moderate but it then drastically increases up to $\overline{\eta}_{lag}/\delta\eta_{oc}^{tide} = 1$, which corresponds to a situation when the mean level of the lagoon reaches the level of the ocean when the tide is at its maximum amplitude. At this WL, the tide amplitude in the lagoon is about half the maximum amplitude reached when there is no river discharge. For $\overline{\eta}_{lag}/\delta\eta_{oc}^{tide} \geq 1$ tide amplitude slowly decreases.

Figure 9 represents $\delta\eta_{lag}^{tide}$, obtained numerically, as a function of both the ocean tide amplitude $\delta\eta_{oc}^{tide}$ and the river flux Q^{riv} . As discussed above, for

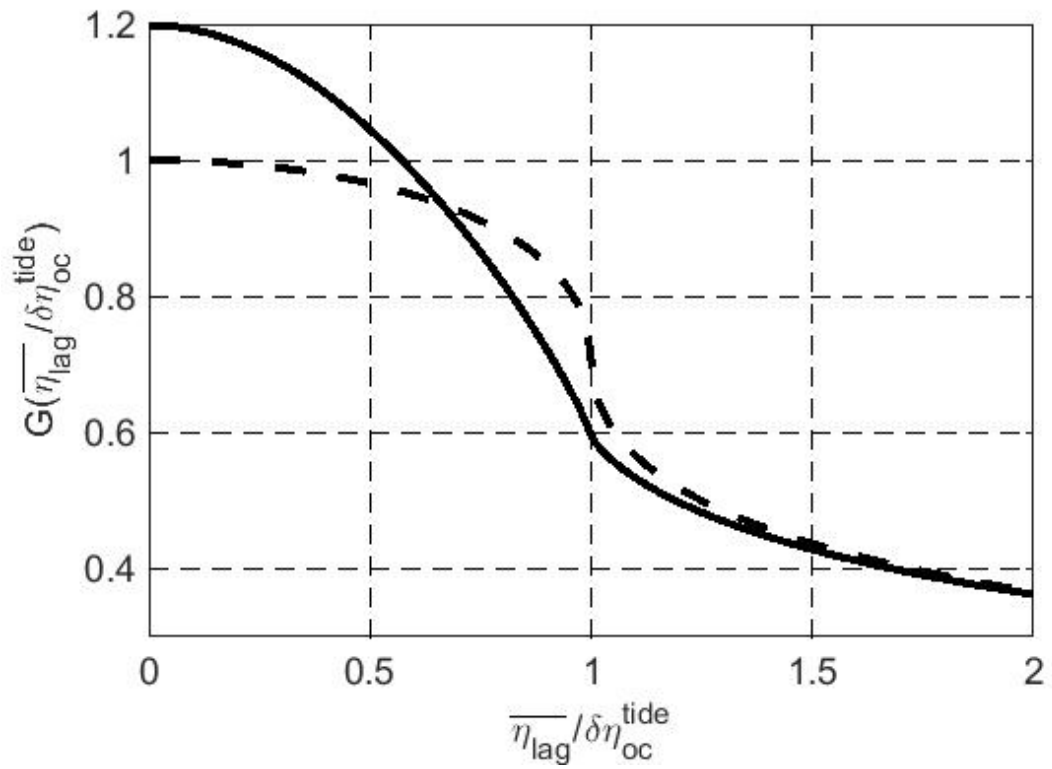


Figure 8: Damping function G (thick line) as a function of $\overline{\eta}_{lag} / \delta \eta_{oc}^{tide}$. The dashed line corresponds to an approximation (see appendix A).

a given ocean tide amplitude, $\delta\eta_{lag}^{tide}$ continuously decreases with increasing river flux. The decrease of $\delta\eta_{lag}^{tide}$ is first relatively weak, then the damping is much stronger up to a critical value for Q^{riv} when the mean level of the lagoon reaches the ocean tide. Above this threshold, the tide amplitude damping is significantly weaker. This explains why, during periods of high river discharge, we observe a strong reduction of the tidal signal in the numerical experiments of the Nokoué Lagoon with simplified tidal and river inflow forcings (see Fig. 4 and 5). Figure 5 represents the analytical (gray curve) and numerical (dashed black curve) solutions, showing excellent agreement. Considering the typical tide off Cotonou, the tidal amplitude in the Nokoué Lagoon remains similar up to a river discharge of $Q^{riv} \simeq 400m^3/s$ (reached after 120 days of simulation). It is then strongly damped for river discharge varying between 400 and 900 m^3/s (reached after 150 days of simulation). For river discharge higher than 900 m^3/s , the tide amplitude in the lagoon oscillates around 2 cm (Fig. 5).

Finally, a phase shift between the tide signal in the lagoon and in the ocean is evident (Fig. 3). This can be explained by the fact that the sign of the flux in the channel (or U) is given by the difference between the levels of the ocean and of the lagoon (see Eq. 1b and Stigebrandt, 1980). The ebb and flood turnovers are thus determined by the reversal of the ocean and lagoon levels, which also correspond to maxima and minima of the lagoon level, as can be seen from Fig. 3. The phase shift between ocean and lagoon tides ϕ depends on the ratio of the tidal amplitudes in the lagoon and the ocean, and is approximately given by (Stigebrandt, 1980):

$$\phi = \frac{\pi}{2} - \frac{\delta\eta_{lag}^{tide}}{\delta\eta_{oc}^{tide}} \quad (12)$$

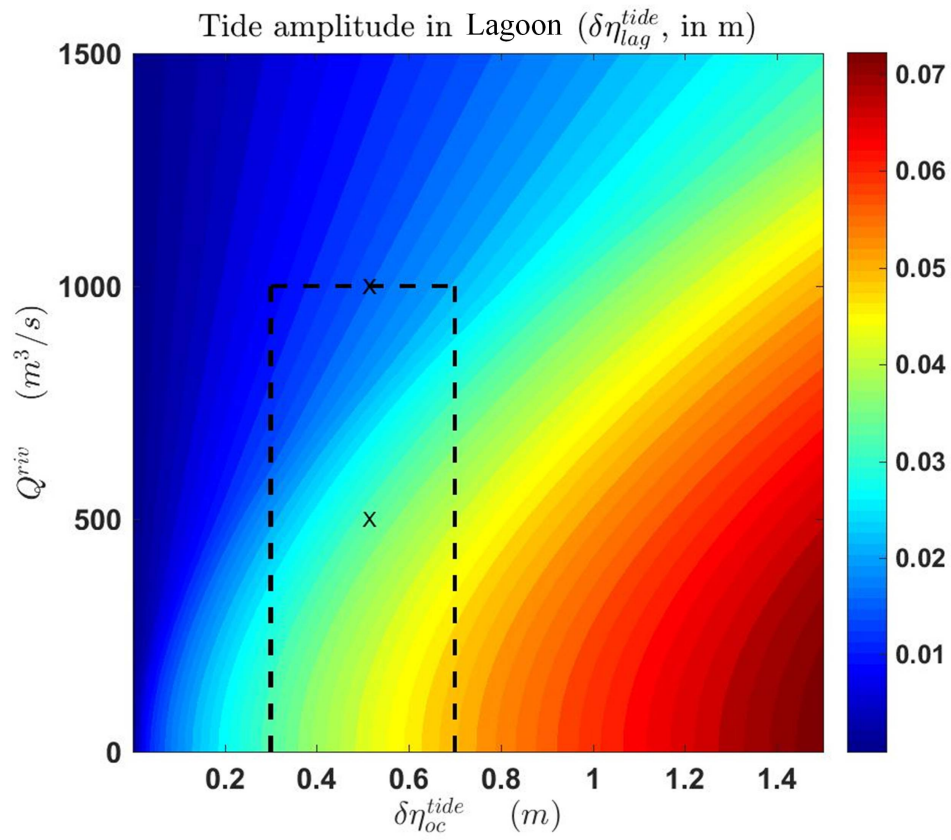


Figure 9: High frequency, tidal, variation of the lagoon WL $\delta\eta_{lag}^{tide}$ given by Eq. 11 for the Nokoué Lagoon characteristics: $\Gamma = 7.10^{-6} m^{1/2}/s$, $A = 1.7 \cdot 10^8 m^2$.

When river discharge is considered, this phase shift also explains the asymmetry of ebb and flood durations. Indeed, the level in the lagoon oscillates around its mean level $\overline{\eta_{lag}}$. This shifts the η_{lag} curve toward higher values and the crossing with the η_{oc} curve is no longer regular. As a result, ebb is longer than flood (see Fig. 3). This simple explanation is however not exact and, strictly speaking, it is only valid when there is no, or weak, river flux. For instance Fig. 3 shows that with strong river flux, ebb and flood cycles are again symmetric and of similar duration. Asymmetry between flood and ebb phases when there exists a river flux is thus more subtle. In this case, as discussed above, the mean level of the lagoon increases and nonlinear interactions between river flux and tide variations determine the mean level. Oscillations around this mean level remain present, associated with tidal forcing. The ebb and flood phases in the lagoon are given by the sign of $\frac{d\eta_{lag}}{dt}$. Using Eq. 9 and 6, Eq. 2 can be rewritten as:

$$\frac{d \delta\eta_{lag}^{tide}}{dt} = \Gamma \left(\sqrt{\overline{\eta_{lag}^{riv}}} + \epsilon \sqrt{|\eta_{oc} - \overline{\eta_{lag}} - \delta\eta_{lag}^{tide}|} \right), \quad (13)$$

which can be used to show that $\frac{d\eta_{lag}}{dt}$ changes sign when

$$\eta_{oc} = \delta\eta_{lag}^{tide} + (\overline{\eta_{lag}} - \overline{\eta_{lag}^{riv}}). \quad (14)$$

Thus the shift to be used when evaluating the crossing between η_{oc} and $\delta\eta_{lag}^{tide}$ curves is not $\overline{\eta_{lag}}$, but $\overline{\eta_{lag}} - \overline{\eta_{lag}^{riv}}$. As $\overline{\eta_{lag}} = \overline{\eta_{lag}^{riv}}$ when the river flux becomes large, the ebb and flood duration asymmetry has to reach a maximum for moderate river flux values and then tend to equal durations. Assuming that $\overline{\eta_{lag}} - \overline{\eta_{lag}^{riv}} \ll \eta_{oc}$ and that the tide amplitude ($\delta\eta_{lag}^{tide}$) is small in the lagoon, the difference between ebb and flood durations can be estimated by

$$\Delta T_{e-f} = 4 \frac{\overline{\eta_{lag}} - \overline{\eta_{lag}^{riv}}}{\omega \eta_{oc}}. \quad (15)$$

Figure 10 represents ΔT_{e-f} as a function of Q^{riv} and η_{oc} . Note it is always positive, ie ebb tides are always longer than flood tides.

For the simplified characteristics presented in section 3.1, the mean tide amplitude is $0.5 m$. The maximum tide asymmetry is reached for a river flux of $Q^{riv} \simeq 500 m^3/s$ and is about $2h40'$, close to what is found (Fig. 3 blue curve). Finally, the approximation of function G plotted in Fig. 8 is valid only when the tide signal can be considered symmetric (see appendix A.2). Thus, symmetry is recovered for the lagoon tide when both curves match, which happens when $\overline{\eta_{lag}} \geq 1.2 \delta\eta_{oc}^{tide}$ (see Fig. 8), which also corresponds to a river flux $Q^{riv} \simeq 900 m^3$ (asymmetry and symmetry of the blue and red curves, Fig. 3).

4.3. Physics of the interaction between tidal and river forcings

The damping of the tide signal in the lagoon is a result of bottom friction within the channel (Stigebrandt, 1980; Hill, 1994; MacMahan et al., 2014). Without river inflow, the amplitude of the tide in the lagoon ($\delta\eta_{lag}^{tide}$) is $1.2 \Gamma \sqrt{\delta\eta_{oc}^{tide}}/\omega$ and is determined by the geometrical characteristics of the channel and bottom friction. Large dissipation in the channel leads to small Γ , and strongly damped tide signal.

We have particularly highlighted the nonlinear interaction between the high-frequency tide forcing and the low-frequency river forcing on the lagoon WL, which leads to a systematic increase of the mean WL and a signature of the neap-spring tidal cycle on the WL. This phenomenon is associated with the increase of average bottom friction coefficient when tide is taken into account. Indeed, the friction coefficient is proportional to $|\overline{U}|$. Without tide, $U = U(Q^{riv})$ is prescribed by the river flux and $|\overline{U}| = |U(Q^{riv})|$. When tide

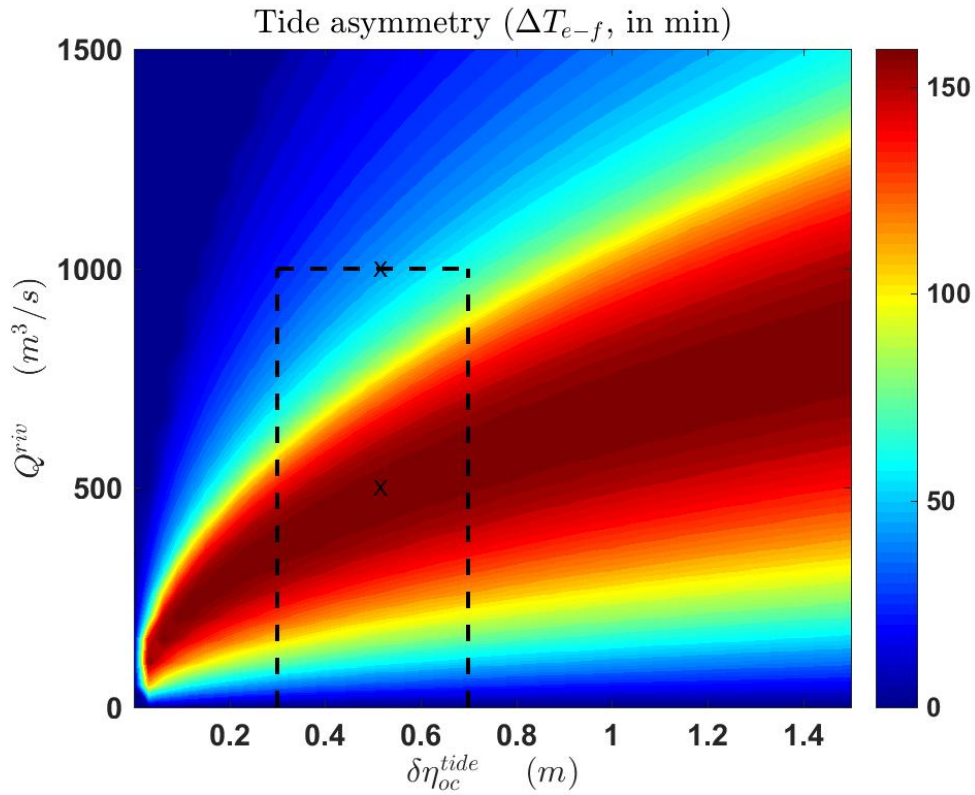


Figure 10: Difference between ebb and flood duration (in minutes) as a function of the ocean tide amplitude and river flux, for the Nokoué Lagoon characteristics: $\Gamma = 7.10^{-6} m^{1/2}/s$, $A = 1.7 \cdot 10^8 m^2$. It is always positive and, for a given tide amplitude, it reaches a maximum of almost 2 hours for intermediate values of the river flux.

is taken into account, $U = \bar{U} + \delta U^{tide}$, where $\overline{U^{tide}} = 0$. Necessarily (because we assume mean equilibrium) $\bar{U} = U(Q^{riv})$ is still driven by the river flux, whatever the tide amplitude. Since $|\overline{U}| > |\bar{U}|$, we get $|\overline{U}| \geq |U(Q^{riv})|$ or higher average dissipation. To maintain equilibrium, this increase of dissipation in the channel requires an increased potential energy (or pressure gradient) and thus an increased WL in the lagoon, in comparison with the “no tide” case. Also, the stronger the oceanic tide, the stronger the dissipation amplification, which explains the signature of the neap-spring tidal cycle on the mean level of the lagoon. Finally note that if $|U(Q^{riv})| > \delta U^{tide}$ (corresponding to the case when the mean lagoon WL is higher than the tide amplitude), we recover $|\overline{U}| = |U(Q^{riv})|$, so that the amplification of friction and mean WL must eventually decrease and disappear for high enough river fluxes, as shown by our numerical results.

5. Estimation of the river inflow to Nokoué Lagoon

In the present Section, we perform a numerical simulation of the observed lagoon WL. The goal is to evaluate if the simplified Stigebrandt (1980) equations can reproduce the observations presented in Fig. 1. Equations 2 are thus forced by realistic oceanic tides and the total river flux estimated for the Nokoué Lagoon in 2018 and 2019. As the latter is not measured, we here derive a method to evaluate it from observations of mean WL evolution in the lagoon, based on the previous analytical results. As mentioned earlier, it is also necessary to estimate the value of the parameter Γ associated with the channel connecting Nokoué lagoon to the ocean. This is done using observations of fluxes in the channel.

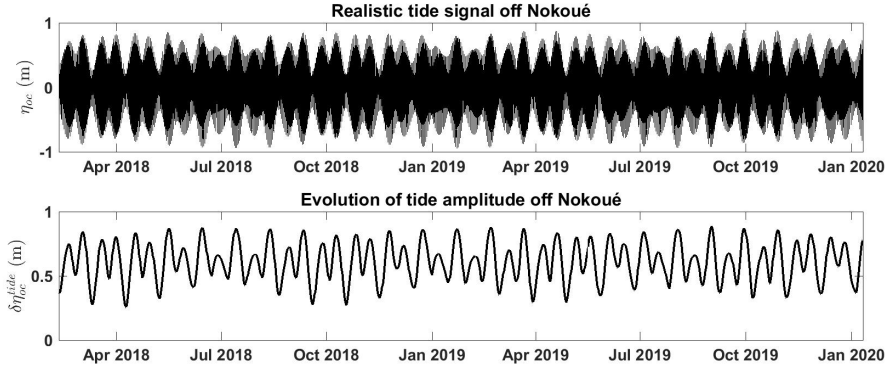


Figure 11: Variation of the sea level associated with tides off Cotonou (results from FES tidal model). Total tide signal (upper panel) and tide amplitude (lower panel).

5.1. Ocean elevation variations

The ocean tide is provided by the FES tide model which assimilates available tide gauges and altimetric products (Lyard et al., 2006). Comparison with the available data over 2018/2019 shows very good agreement, with error of the order of 2% for the tide amplitude (Chaigneau et al., 2022). Figure 11 shows the ocean tide signal and tide amplitude for the time period of observation of the Nokoué Lagoon. The tide amplitude varies from about 25 *cm* to almost 90 *cm*. The amplitude for the principal frequencies M2, S2 and K1 are respectively 0.50 *m*, 0.18 *m* and 0.13 *m* and M2 is the main frequency.

5.2. Estimate of parameters

In order to build a numerical solution using the simplified Stigebrandt (1980) model, we need to know the evolution of the elevation in the ocean and of the total river inflow to Nokoué Lagoon. Unfortunately, the river discharge is currently not monitored, which is problematic, since it drives

the mean level of the lagoon. However, we can use the analytical model derived here to estimate this net river discharge. Indeed, the mean level of the lagoon is directly linked to the river flux, and using Eq. 10 and 9, we can write

$$Q^{riv} = \Gamma A \sqrt{\delta\eta_{oc}^{tide}} F\left(\frac{\overline{\eta}_{lag}}{\delta\eta_{oc}^{tide}}\right) \quad (16)$$

We consider Γ is constant and first use Eq. 16 to evaluate ΓA (and thus Γ) from a few estimates of the mean fluxes in the channel, inferred from ADCP data. Then, considering the estimated value of ΓA , the low-frequency river discharge is reconstructed from Eq. 16, using direct observations of the WL in the lagoon from a pressure sensor and of the tide amplitude in the ocean from FES.

Figure 12 shows the relationship between the measured mean fluxes (obtained from the 14 ADCP campaigns), and the values of the $\sqrt{\delta\eta_{oc}^{tide}} F\left(\frac{\overline{\eta}_{lag}}{\delta\eta_{oc}^{tide}}\right)$ term in Eq. 16, estimated from the measured mean level in the lagoon and ocean tide amplitude taken at the time of the ADCP campaigns. Although the uncertainties of the observed mean fluxes values can be large during the dry season, when the river discharge is weak and tide fluxes relatively strong in the channel, we note a clear linear relationship between the observed and estimated mean fluxes. This correlation leads to an estimated value of $\Gamma A \simeq 1200 \text{ m}^5/2/s$ (see Fig. 12) and considering a lagoon area $A = 1.7 \cdot 10^8 \text{ m}^2$, we obtain:

$$\Gamma \simeq 7.10^{-6} \text{ m}^{1/2}/s \quad (17)$$

Note that alternative methods can be used to evaluate Γ from the observation of the tide amplitude in the lagoon and in the ocean. For instance

according to Eq. 11, a bulk estimate for Γ is given by

$$\Gamma \simeq \frac{\omega_{M2} [\delta\eta_{lag}^{tide}]}{1.2 [\sqrt{\delta\eta_{oc}^{tide}} G(\overline{\eta}_{lag}/\delta\eta_{oc}^{tide})]} \quad (18)$$

where the symbol $[\cdot]$ denotes the temporal mean taken over the entire time period of observation. This yields $\Gamma \simeq 6.84 \cdot 10^{-6} \text{ m}^{1/2}/\text{s}$ (or $\Gamma A = 1170 \text{ m}^{5/2}/\text{s}$), very close to the value obtained above.

Figure 13 shows the net river discharge estimated using Eq. 16 and 17, and $\Gamma A \simeq 1200 \text{ m}^{5/2}/\text{s}$. This reconstructed time series shows that over the study period, the maximum river discharge was of $Q^{riv} \simeq 1100 \text{ m}^3/\text{s}$ in November 2019. Such high values of river flux have been obtained from models of the Ouémé watershed (Lawin et al., 2019). Unsurprisingly, there is a strong annual variability and much more water has been drained into the lagoon in the wet season of 2019 than in 2018. From our estimates of the river flux, the cumulative volume of fresh water entering the lagoon from the 1st of July to the 31st of December amounts to $5.2 \cdot 10^9 \text{ m}^3$ in 2018 and $8.3 \cdot 10^9 \text{ m}^3$ in 2019.

Weak negative values ($< -50 \text{ m}^3/\text{s}$), observed episodically during the dry season of 2018, could be associated with processes not considered here. For instance, given the lagoon and air characteristics, a mean evaporation rate of about $5 \text{ mm}/\text{day}$ is a realistic order of magnitude, as reported on other tropical lakes around the world (Moniod, 1973; Colleuil, 1987; de Farias Mesquita et al., 2020). Given the lagoon area, this gives a negative water flux of $-10 \text{ m}^3/\text{s}$. Since, during the dry season, the river fluxes from historical observations are within $20 - 50 \text{ m}^3/\text{s}$ (Djihouessi and Aina, 2018; Okpeitcha et al., 2022; Chaigneau et al., 2022), we conclude that other processes, such as reflows recharging groundwaters or the wetlands, or low frequency ocean

variations (decrease of the mean ocean water level in this area), have to be considered to refine our estimates during the dry season. However, the negative peaks are not strong artifacts, so we will not discuss them further here or filter them out in the following simulation.

5.3. Reconstruction of the WL in the Nokoué Lagoon and comparison with observations

Equation 2 is now solved using the ocean tide forcing from FES and the estimated river discharge (see Fig. 13). Note this is not a circularity, even though the river fluxes have been reconstructed from the observed mean WL. Indeed, from the 14 observations presented in Fig. 12 only 4 observations, associated with very high river fluxes, are used to calibrate the model and calculate Γ (Fig. 12) and we only know the model will give good results for these 4 specific events. Confronting our results to the observations for the whole time periods of 2 years, will confirm that the simplified model correctly represents the physics of the WL variations in the lagoon. In particular, this model considers a constant value for Γ , determined by the physical properties of the channel.

Figure 14 presents our results. The total signal (upper panel, which can be compared to the observed total signal in Fig. 1) is decomposed into mean WL variations (middle panel) and tide amplitudes (lower panel) for both the observations (gray line) and numerical solution (black line). The computed WL follows the observations quite closely, in particular for the neap/spring tide variability. The RMSE is about 4 *cm* and maximum differences do not exceed 10 *cm*. Note also that the computed maximum WL occurring in October 2018 and November 2019 are close to the observations, but are

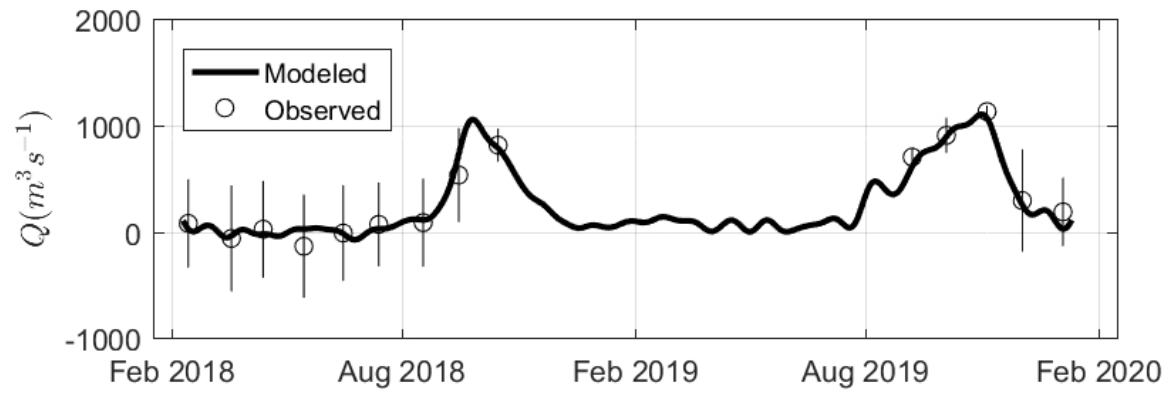


Figure 13: Estimated evolution of the total river flux in Nokoué Lagoon (plain line). The mean fluxes observed in the channel and associated with the river inflow are plotted as circles with error bars.

reached with a few day lag in the model.

Stronger discrepancies are observed for the tide amplitude signals. Indeed the model tends to overestimate the tide amplitude during neap-tide periods, in particular from May to August. The model agrees better with the observations when the tide amplitude reaches a minimum during the wet season, due to a high river discharge (e.g. sections 3 and 4.2 and Fig. 5). The discrepancy at the beginning of the wet season is unclear and may be associated with seasonal variability. As indicated above, there exists some low frequency -seasonal- variability of the wind, or of the ocean level, that would have to be taken into account. Finally, the model considers a mean tide signal over the whole lagoon, whereas tide dynamics within the lagoon can also lead to differences and stronger variations between spring and neap tides close to the channel entrance where the observations are taken.

Finally, another difference is that there exists a phase shift between the spring/neap tide cycle in the observations and in the model (Fig. 14, bottom panel). In fact, the model exhibits minima and maxima of the tide amplitude in phase with the ocean. The observations exhibit a lag of 3 to 4 days, likely associated with nonlinear effects involving processes that are not considered within the present framework and discussed in the concluding section.

6. Discussion and conclusion

We have analyzed the dynamics of a choked lagoon constrained by both the ocean tide and river inflow. The interaction of the high frequency, tidal, and low frequency, river, forcings are nonlinear, which leads to striking effects such as a strong signature of the neap-spring tidal cycle on the mean

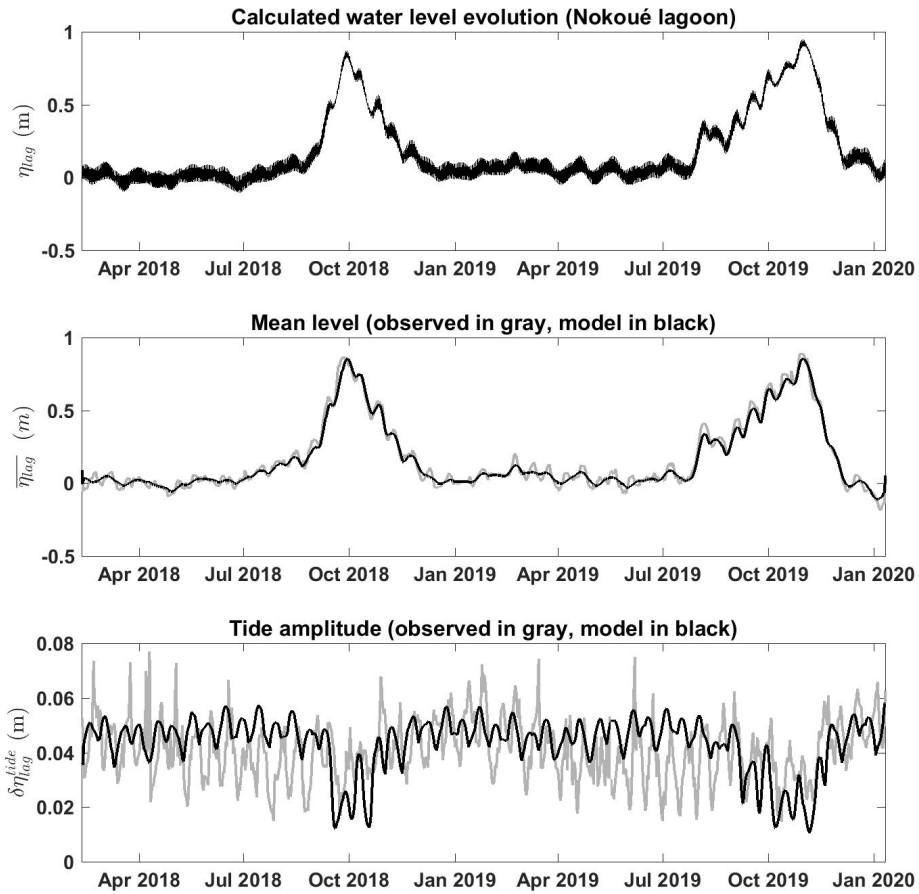


Figure 14: Top panel : total variations of the WL in Nokoué Lagoon from the model. Middle panel : mean level evolution for the observations (gray curve) and from the numerical solution (black curve). Lower panel : evolution of the tidal amplitude in the lagoon for the observations (gray curve) and for the numerical solution (black curve).

level of the lagoon, in particular when there is a strong river discharge into the lagoon. Approximate analytical solutions have been developed, based on the Stigebrandt (1980) equations, which are simplified but reliable in many circumstances for choked channels (Stigebrandt, 1992). The analytical solutions represent very well the major features of the observations. It has thus been used to explain the physics of the nonlinear interactions. We have shown that the mean level in the lagoon depends on tides and that submer-sion risks, associated with strong river fluxes, are much higher during spring tides. Even though specific applications were made using the Nokoué Lagoon characteristics, the analytical solution and described processes are valid for any choked lagoon and the influence of river fluxes on the lagoon mean WL and tide amplitude can be evaluated provided the lagoon area A and the channel choking coefficient Γ can be estimated.

Finally, we propose a method to calibrate ΓA from a small number of observations of the mean channel flux. The analytical solution then permits deriving the net river flux to the lagoon, from the ocean and mean lagoon WL only. This has been applied to Nokoué Lagoon, for which river flux observations are rare in recent years. ΓA was estimated using the analytical solution and 14 discharge measurements in the Cotonou channel. An estimated net river flux was then obtained at high frequency. The obtained model was then applied to a 2 year time period, reproducing the mean WL variations. The computed tide amplitude in the lagoon is also satisfactory: the order of magnitude is well reproduced but there are discrepancies in the spring/neap tide and seasonal variability and a time lag of 3-4 days between the temporal amplitude modulation in the model and the observations. This

effect has been specifically studied in Hill (1994) (see also MacMahan et al., 2014) and is attributed to nonlinear interactions when the effect of ocean tide WL variation is considered to estimate the WL in the channel (Eq. 3). When the ocean tide amplitude is comparable to the mean channel depth, this effect was shown to generate a spring-neap mean WL variation in the lagoon. We did not consider this effect here as i) we wanted to focus on the interaction between ocean tides and river fluxes, ii) in the case of Nokoué Lagoon, the ocean tide is smaller than the channel depth. However, Hill (1994) has shown that this effect also generates a lag of the temporal amplitude modulation between the lagoon and the ocean, reaching up to three days. It is thus possible that a similar lag can be achieved in our configuration, provided the modification of the channel depth by the ocean tide and river flux are taken into account.

Additional perspectives can be proposed to improve the understanding and predictive possibilities of the model. For instance, it seems interesting to take into account evaporation, reflows recharging groundwaters or the wetlands, or the low frequency variations of the ocean level (associated with coastal waves, the effect of the wind or of the large scale circulation on the WL at the coast). Note that forcing by river fluxes or ocean level do not intervene similarly in Eq. 2 so that new effects can be expected.

The influence of stratification due to density difference between the salty ocean and the brackish (sometimes fresh) water of the lagoon has not been considered. This generates an additional pressure gradient that significantly affects the fluxes in the channel in particular during the dry season (Okpeitcha et al., 2022).

A possible explanation for the seasonal variations of the tide signal observed in the lagoon (and the discrepancy with the model), might be the variation of the atmospheric tide at seasonal period. Indeed, observations indicate a relatively strong atmospheric tide signal in the atmospheric pressure in this area, with an amplitude possibly varying seasonally from 1 to 2 mbar (Dai and Wang, 1999) and a phasing with the ocean tide that can also vary.

Tides are also known to influence the water level in rivers from estuaries to far upriver. Nonlinear interactions of different tide constituents, associated with bottom friction and the effect of the river flux variations, are known to play a role in the variation of the water level and tidal asymmetries at subtidal frequencies (Jay and Flinchem, 1997; Guo et al., 2015, 2019). It is however not clear at this stage if the present analytical results can be generalized to river dynamics, since additional processes, such as convergence effect associated with the variations of the river width and depth, have to be considered too.

Finally, simple operational systems for the variations of the WL in lagoons, in combination with the analysis presented here, can be of interest for flooding alerts. In this case observations of river fluxes are necessary, far upstream of the lagoon. Fluxes can be derived from the knowledge of the river WLs and, for the Nokoué Lagoon, we could correlate historical observations of river WLs and estimated river fluxes obtained with our model. Many African countries are not equipped with efficient in situ operational systems for the observation of river WLs, but altimetric satellite data is now available for many rivers (see <https://www.theia-land.fr/en/hydroweb/>), in particular

Ouémé. Currently the altimetric satellite cycle is too low (about 10 days at best) to provide operational observations. But project of altimetric satellite constellations with a revisit frequency of about 1 day are currently discussed (International-Altimetry-Team, 2021).

Acknowledgments

The authors thank contributions from IRD (Institut de Recherche pour le Développement) through the long term program JEAI-SAFUME (salt and freshwater variability at multiscale, from Tropical Atlantic to lagoon systems), ANR @RAAction chair medLOC (ANR-14-ACHN- 0007-01 T. Stieglitz) and OmiDelta project (V. Okpeitcha PhD grant), funded by the Netherlands government. This study is also part of the project "lagune Nokoué" funded by CNES/TOSCA. Suggestion of a reviewer drastically improved section 4.3 and also led to the discussion on the influence of evaporation in the concluding section.

A. Approximate solution with tidal forcing

A.1. Approximate solution for mean lagoon WL

Assuming that the tidal variation in the lagoon $\delta\eta_{lag}^{tide}$ can be neglected in comparison with the oceanic signal $\delta\eta_{oc}^{tide}$ in the right hand side term of Eq. 2, we average Eq. 2 over one tidal period $T = 2\pi/\omega$ (considering that both the oceanic tide amplitude $\delta\eta_{oc}^{tide}$ and the river flux Q^{riv} are constant over this time period) to get

$$\frac{1}{T} \int_0^T \frac{\overline{\eta_{lag}} - \delta\eta_{oc}^{tide} \sin\omega t}{\sqrt{|\overline{\eta_{lag}} - \delta\eta_{oc}^{tide} \sin\omega t|}} dt = \frac{Q^{riv}}{\Gamma A} \quad (19)$$

Setting $\theta = \omega t$, using Eq. 9 and with simple calculations, we obtain

$$F(\overline{\eta}_{lag}/\delta\eta_{oc}^{tide}) = \frac{1}{2\pi} \int_0^{2\pi} \frac{\overline{\eta}_{lag}/\delta\eta_{oc}^{tide} - \sin\theta}{\sqrt{|\overline{\eta}_{lag}/\delta\eta_{oc}^{tide} - \sin\theta|}} d\theta = \sqrt{\frac{\overline{\eta}_{lag}^{riv}}{\delta\eta_{oc}^{tide}}} \quad (20)$$

that we invert to get

$$\overline{\eta}_{lag} = F^{-1}\left(\sqrt{\frac{\overline{\eta}_{lag}^{riv}}{\delta\eta_{oc}^{tide}}}\right) \delta\eta_{oc}^{tide} \simeq \begin{cases} 1.2 \sqrt{\overline{\eta}_{lag}^{riv} \delta\eta_{oc}^{tide}} & \text{if } \sqrt{\overline{\eta}_{lag}^{riv}/\delta\eta_{oc}^{tide}} \rightarrow 0 \\ \overline{\eta}_{lag}^{riv} & \text{if } \sqrt{\overline{\eta}_{lag}^{riv}/\delta\eta_{oc}^{tide}} \rightarrow \infty \end{cases} \quad (21)$$

The approximate solution in Eq. 21 can be obtained from approximate forms of the function F defined in Eq. 20. Indeed, when $\overline{\eta}_{lag}/\delta\eta_{oc}^{tide}$ is small, trivial manipulations show that the integral in Eq. 20 reduces to

$$F(\overline{\eta}_{lag}/\delta\eta_{oc}^{tide}) = \frac{1}{\pi} \int_0^\pi \frac{\overline{\eta}_{lag}/\delta\eta_{oc}^{tide}}{2\sqrt{\sin\theta}} d\theta \simeq 0.83 \overline{\eta}_{lag}/\delta\eta_{oc}^{tide} \quad (22)$$

When $\overline{\eta}_{lag}/\delta\eta_{oc}^{tide}$ is large, it is simply

$$F(\overline{\eta}_{lag}/\delta\eta_{oc}^{tide}) = \frac{1}{2\pi} \int_0^{2\pi} \sqrt{\overline{\eta}_{lag}/\delta\eta_{oc}^{tide}} d\theta = \sqrt{\overline{\eta}_{lag}/\delta\eta_{oc}^{tide}} \quad (23)$$

This yields the approximations for F^{-1} and the asymptotic form given in Eq. 21. Figure 6 shows F^{-1} and its approximations.

A.2. Approximate solution for tidal signal

Using Eq. 6 into 2 and again neglecting $\delta\eta_{lag}^{tide}$ (typically of few centimeters) in front of $\delta\eta_{oc}^{tide}$ (50 cm off Cotonou) we get

$$\frac{d(\delta\eta_{lag}^{tide} s)}{dt} = \Gamma \frac{\delta\eta_{oc}^{tide} \sin \omega t - \overline{\eta}_{lag}}{\sqrt{|\delta\eta_{oc}^{tide} \sin \omega t - \overline{\eta}_{lag}|}} + \frac{Q^{riv}}{A} \quad (24)$$

Using Eq. 19, we get

$$\frac{d(\delta\eta_{lag}^{tide} s)}{dt} = \Gamma \sqrt{\delta\eta_{oc}^{tide}} \left[\frac{\sin \omega t - \overline{\eta}_{lag}/\delta\eta_{oc}^{tide}}{\sqrt{|\sin \omega t - \overline{\eta}_{lag}/\delta\eta_{oc}^{tide}|}} - F(\overline{\eta}_{lag}/\delta\eta_{oc}^{tide}) \right] \quad (25)$$

and finally

$$\delta\eta_{lag}^{tide} s = \frac{\Gamma \sqrt{\delta\eta_{oc}^{tide}}}{\omega} \int_0^{\omega t} \left[\frac{\sin \theta - \overline{\eta_{lag}}/\delta\eta_{oc}^{tide}}{\sqrt{|\sin \theta - \overline{\eta_{lag}}/\delta\eta_{oc}^{tide}|}} - F(\overline{\eta_{lag}}/\delta\eta_{oc}^{tide}) \right] d\theta \quad (26)$$

This gives a solution for the periodic function s for the tidal signal in the lagoon, and the following expression for the amplitude $\delta\eta_{lag}^{tide}$:

$$\delta\eta_{lag}^{tide} = \frac{\Gamma \sqrt{\delta\eta_{oc}^{tide}}}{\omega} G(\overline{\eta_{lag}}/\delta\eta_{oc}^{tide}) \quad (27)$$

where G is the amplitude of the variation of the periodic function s and is given by:

$$G(\overline{\eta_{lag}}/\delta\eta_{oc}^{tide}) = \frac{1}{2} \Delta_{max-min} \left[\int_0^\theta \left[\frac{\sin \theta - \overline{\eta_{lag}}/\delta\eta_{oc}^{tide}}{\sqrt{|\sin \theta - \overline{\eta_{lag}}/\delta\eta_{oc}^{tide}|}} - F(\overline{\eta_{lag}}/\delta\eta_{oc}^{tide}) \right] d\theta \right] \quad (28)$$

where $\Delta_{max-min}[\cdot]$ represents the variation (maximum - minimum) of the function. We were not able to give an analytical expression for G in the general case, but the function can be easily evaluated numerically and Fig. 8 shows its general shape.

An explicit approximate solution can also be given, starting from Eq. 25 and assuming that s is close to \sin so that its derivative is close to \cos . This corresponds to neglecting the asymmetry of the tide signal and is generally a strong approximation except when the river flux is so strong that the mean level of the lagoon reaches the oceanic tide amplitude (see Fig. 10). $\delta\eta_{lag}^{tide}$ can then be evaluated using the amplitude (maximum value - minimum value) of the left hand side of Eq. 25 and we get

$$G_{approx}(\overline{\eta_{lag}}/\delta\eta_{oc}^{tide}) = \frac{1}{2} \begin{cases} \sqrt{1 + \overline{\eta_{lag}}/\delta\eta_{oc}^{tide}} + \sqrt{1 - \overline{\eta_{lag}}/\delta\eta_{oc}^{tide}} & \text{if } \overline{\eta_{lag}}/\delta\eta_{oc}^{tide} \leq 1 \\ \sqrt{1 + \overline{\eta_{lag}}/\delta\eta_{oc}^{tide}} - \sqrt{\overline{\eta_{lag}}/\delta\eta_{oc}^{tide} - 1} & \text{if } \overline{\eta_{lag}}/\delta\eta_{oc}^{tide} \geq 1 \end{cases} \quad (29)$$

G_{approx} is represented as the dashed line in Fig. 8. It is only precise and useful when $\overline{\eta_{lag}}/\delta\eta_{oc}^{tide} \geq 1.2$ or so, and it then decreases as $1/2\sqrt{\overline{\eta_{lag}}/\delta\eta_{oc}^{tide}}$.

References

- Ahouangan, M., Djaby, B., Ozer, P., Hountondji, Y., Thiry, A., Longueville, F. D., 2014. Adaptation et résilience des populations rurales face aux catastrophes naturelles en Afrique subsaharienne. Cas des inondations de 2010 dans la commune de Zagnanado, Bénin. In: Ballouche, A. & Taibi, N. A. (Eds.), Eau, milieux et aménagement. Une recherche au service des territoires. Presses de l'Université d'Angers, Angers, France., 265-278.
- Albrecht, N., Vennell, R., 2007. Tides in two constricted new zealand lagoons. New Zealand Journal of Marine and Freshwater Research 41 (1), 103–118.
- Biao, E. I., 2017. Assessing the impacts of climate change on river discharge dynamics in oueme river basin (benin, west africa). Hydrology 4 (4).
URL <https://www.mdpi.com/2306-5338/4/4/47>
- Chaigneau, A., Okpeitcha, O. V., Morel, Y., Stieglitz, T., Assogba, A., Benoist, M., Allamel, P., Honfo, J., Awoulmbang Sakpak, T. D., Rétif, F., Duhaut, T., Peugeot, C., Sohou, Z., 2022. From seasonal flood pulse to seiche: Multi-frequency water-level fluctuations in a large shallow tropical lagoon (nokou lagoon, benin). Estuarine, Coastal and Shelf Science 267, 107767.
- Colleuil, B., 1987. Le complex lagunaire du lac nokoué et de la lagune de porto novo (benin). In: Burgis, M.J., Symoens, J.J., Gac, J.Y. (Eds.), African Wetlands and Shallo Water, 211, ORSTOM, Pais, 188–196.

- Dai, A., Wang, J., 1999. Diurnal and semidiurnal tides in global surface pressure fields. *Journal of the Atmospheric Sciences* 56 (22), 3874–3891.
- de Farias Mesquita, J. B., Lima Neto, I. E., Raabe, A., de Arajo, J. C., 2020. The influence of hydroclimatic conditions and water quality on evaporation rates of a tropical lake. *Journal of Hydrology* 590, 125456.
- Djihouessi, M. B., Aina, M. P., 2018. A review of hydrodynamics and water quality of lake nokoué: Current state of knowledge and prospects for further research. *Regional Studies in Marine Science* 18, 57 – 67.
- Djihouessi, M. B., Aina, M. P., Kpanou, B., Kpondjo, N., 2017. Measuring the total economic value of traditional sand dredging in the coastal lagoon complex of grand-nokoué (benin). *Journal of Environmental Protection* 8, 1605–1621.
- FAO, 2008. Profils des pêches et de laquaculture par pays : vue générale du secteur des pêches national de la république du Bénin. Food and Agriculture Organization of the United Nation. Report FID/CP/BEN, Available in: http://www.fao.org/fishery/docs/DOCUMENT/fcp/fr/FLCP_BJ.pdf (last access: October 10, 2021).
- Guo, L., van der Wegen, M., Jay, D. A., Matte, P., Wang, Z. B., Roelvink, D., He, Q., 2015. River-tide dynamics: Exploration of nonstationary and non-linear tidal behavior in the yangtze river estuary. *Journal of Geophysical Research: Oceans* 120 (5), 3499–3521.
- Guo, L., Wang, Z. B., Townend, I., He, Q., 2019. Quantification of tidal

- asymmetry and its nonstationary variations. *Journal of Geophysical Research: Oceans* 124 (1), 773–787.
- Hill, A., 1994. Fortnightly tides in a lagoon with variable choking. *Estuarine, Coastal and Shelf Science* 38 (4), 423 – 434.
- International-Altimetry-Team, 2021. Altimetry for the future: Building on 25 years of progress. *Advances in Space Research* 68 (2), 319–363, 25 Years of Progress in Radar Altimetry.
URL <https://www.sciencedirect.com/science/article/pii/S0273117721000594>
- Jay, D. A., Flinchem, E. P., 1997. Interaction of fluctuating river flow with a barotropic tide: A demonstration of wavelet tidal analysis methods. *Journal of Geophysical Research: Oceans* 102 (C3), 5705–5720.
- Lalèyè, P., Niyonkuru, C., Moreau, J., Teugels, G., 2003. Spatial and seasonal distribution of the ichthyofauna of lake nokoué, bénin, west africa. *African Journal of Aquatic Science* 28 (2), 151–161.
- Latifou, A. B., Toko, I. I., Elegbe, H. A., Pelebe, R., Tougan, P., Boni, A. R., Ahyi, V., Hossou, E. S., Vissiennon, Z., Chikou, A., 2020. Les produits halieutiques au bénin : Sources d'approvisionnement et statistiques. *International Journal of Progressive Sciences and Technologies* 21 (1), 152–167.
- Lawin, A. E., Houngué, R., NTcha MPo, Y., Houngué, N. R., Attogouinon, A., Afouda, A. A., 2019. Mid-century climate change impacts on ouémé river discharge at bonou outlet (benin). *Hydrology* 6 (3).

- Le Barbé, L., Alé, G., Millet, B., Texier, H., Borel, Y., Gualde, R., 1993. Les ressources en eaux superficielles de la République du Bénin. ORSTOM, Paris.
- Lyard, F., Lefevre, F., Letellier, T., Francis, O., Dec 2006. Modelling the global ocean tides: modern insights from fes2004. *Ocean Dynamics* 56 (5), 394–415.
- MacMahan, J., [van de Kreeke], J., Reniers, A., Elgar, S., Raubenheimer, B., Thornton, E., Weltmer, M., Rynne, P., Brown, J., 2014. Fortnightly tides and subtidal motions in a choked inlet. *Estuarine, Coastal and Shelf Science* 150, 325 – 331, special issue on Problems of Small Estuaries.
- Moniod, F., 1973. Régime hydrologique de l’ouémé (dahomey). *Cahiers ORSTOM. Srie Hydrologie* 10 (2), 171–183.
- Newton, A., Brito, A. C., Icelly, J. D., Derolez, V., Clara, I., Angus, S., Schernewski, G., Incio, M., Lilleb, A. I., Sousa, A. I., Béjaoui, B., Solidoro, C., Tosic, M., Caedo-Argelles, M., Yamamuro, M., Reizopoulou, S., Tseng, H.-C., Canu, D., Roselli, L., Maanan, M., Cristina, S., Ruiz-Fernndez, A. C., de Lima, R. F., Kjerfve, B., Rubio-Cisneros, N., Pérez-Ruzafa, A., Marcos, C., Pastres, R., Pranovi, F., Snoussi, M., Turpie, J., Tuchkovenko, Y., Dyack, B., Brookes, J., Povilanskas, R., Khokhlov, V., 2018. Assessing, quantifying and valuing the ecosystem services of coastal lagoons. *Journal for Nature Conservation* 44, 50–65.
URL <https://www.sciencedirect.com/science/article/pii/S1617138117301371>
- Okpeitcha, O. V., Chaigneau, A., Morel, Y., Stieglitz, T., Pomalegni, Y.,

- Sohou, Z., Mama, D., 2022. Seasonal and interannual variability of salinity in a large west-african lagoon (Nokoué lagoon, benin). *Estuarine, Coastal and Shelf Science* 264, 107689.
- Rydberg, L., Wickbom, L., 1996. Tidal choking and bed friction in negombo lagoon, sri lanka. *Estuaries and Coasts* 19 (3), 540–547.
- Stigebrandt, A., 1980. Some aspects of tidal interaction with fjord constrictions. *Estuarine and Coastal Marine Sciences* 11, 151,166.
- Stigebrandt, A., 1992. Bridge-induced flow reduction in sea straits with reference to effects of a planned bridge across resund. *Ambio* 21 (2), 130–134.
- World-Bank, 2011. Inondations au Benin: Rapport d’Evaluation des Besoins Post Catastrophe. World Bank report: Washington, DC, USA. available at <http://documents1.worldbank.org/curated/en/750141468208769683/pdf/694130ESW0P1240loo> (last access: December 24, 2020).